Desalination and Water Treatment
www.deswater.com

doi: 10.5004/dwt.2022.28120

248 (2022) 188–202
February

Adsorption of copper and lead ions from solution by PVDF-PEI blend film

Xiaoting Zhang, Runping Han*

College of Chemistry, Green Catalysis Center, Zhengzhou University, No. 100 of Kexue Road, Zhengzhou 450001, China, emails: rphan67@zzu.edu.cn (R. Han), 1619888517@qq.com (X. Zhang)

Received 17 September 2021; Accepted 30 December 2021

ABSTRACT

A novel film adsorbent (PVDF-PEI) was prepared by simple blending polyethyleneimine and polyvinylidene fluoride for efficient uptake Cu(II) and Pb(II) from solution. The characterization of PVDF-PEI was investigated by Fourier-transform infrared spectroscopy and X-ray photoelectron spectroscopy. Moreover, the effect about adsorbent mass, solution pH, salinity, contact time, temperature and initial Cu(II) and Pb(II) concentrations was researched by batch experiments, respectively. The adsorption quantity of Cu(II) and Pb(II) was to 81.3 and 178 mg g^{-1} from Langmuir model under the solid-liquid ratio was 0.5 g L^{-1} for 8 h at 303 K. Freundlich model and Koble–Corrigan mode well predicted the adsorption isotherms while pseudo-first-order and Elovich models appropriately described the adsorption kinetic curves. The thermodynamic parameters illustrated that both processes were endothermic and spontaneous reactions with increased entropy. Cu-loaded PVDF-PEI and Pb-loaded PVDF-PEI were better regenerated by using 0.1 mol L^{-1} HCl and HNO_3, respectively. The mechanisms were both complexation and ion exchange. Overall, it is referred that PVDF-PEI be promising for eliminating Cu(II) and Pb(II) from wastewater.

Keywords: PVDF-PEI blended film; Adsorption; Copper ion; Lead ion

1. Introduction

As members of the modern metal products development industry, copper and lead still have the potential harm while benefiting mankind. At present, various industrial operations such as metal processing, battery machining, electroplating and dye industry lead to the entry of copper and lead wastewater into water bodies [1,2]. Based on their high toxicity as well as non-biodegradability, they are enriched by animals or plants, further enter the human body and endanger human health, such as dizziness, headaches, stomach aches and kidney damage even under trace conditions [1]. Therefore, the issue of removing copper and lead is a crucial topic in the development of human society.

At present, many ways for removing copper and lead from water have been explored, such as precipitation, adsorption method, film filtration means, ion exchange method as well as solvent extraction technology [3–5]. However, there are still some disadvantages among those methods; for example, the precipitation method and the extraction method are suitable for removing high-concentration heavy metal, the ion exchange method is costly, and so on [6]. The adsorption method is most common for removing heavy metal based on high efficiency, low cost, strong selectivity, simple operation, and high reproducibility [7]. At present, there are still some short part during the common adsorption methods for removing Cu(II) and Pb(II). For example, the adsorption capacity of Cu(II) on grape bagasse activated carbon was 43.47 mg g^{-1} [8]. The maximum uptake capacity of Cu(II)-imprinted polyvinyl alcohol/poly(acrylic acid) films uptake Cu(II) be not reaching 1.28 mmol g^{-1} [9]. The uptake capacity of Pb(II) by surface-modified porous lignin was 188 mg g^{-1} [10]. The adsorption capacity of the porous fly ash geopolymer toward Pb(II) was lower than 6.4 mg g^{-1} [11]. The adsorption capacity of cysteine-functionalized lignin on Pb(II) and

* Corresponding author.

Cu(II) was less than 68.7 mg g^{-1} [12]. Since the adsorption capacity is dominant in the evaluation of the adsorption performance of the material, increasing the uptake capacity of adsorbents is an important direction of research.

However, the use of common powder materials is limited by the difficulty in separation of the spent adsorbent from solution. So the use of adsorptive composite membrane is considered to remove heavy metal ions and other micropollutants from solution through adsorption or filtration [13]. There is much attention about membrane technique due to the synergistic properties of adsorption or filtration approaches. At present, the polyvinylidene fluoride (PVDF) film has attracted much attention in the organic film material during adsorption methods based on its strong heat opposition, oxidation resistance and mechanical behavior [14]. Since the pure PVDF film has strong hydrophobicity (no adsorption to copper and lead in the study) [15], it is necessary to introduce amphiphilic substances to increase its hydrophilicity. However, the hydrophilic modifiication methods of PVDF membrane reported in the past are relatively complex; for example, hydrophilic PVDF membrane prepared by in situ polymerisation and micro-phase separation of 2-hydroxyethyl methacrylate [15]. Polyethyleneimine (PEI) contains a large amount of –NH and $–NH_2$ [16], and can be combined with PVDF, so it has been widely studied by many scholars (used as a modifier) for the removal of contaminants from water and the medicine industries so on. For example, Fan et al. [17] applied graphene oxide modified with PEI as a new antibacterial material for methicillin-resistant *Staphylococcus aureus*. Kani et al. [18] removed anionic dyes by using PEI-modified Tiger nut residue. At the same time, PEI as a strong amphiphilic substance has the characteristics of non-volatile and high chemical stability [19]. Therefore, this topic improved the hydrophilicity of materials by simple introducing PEI in PVDF casting solution, and it had a good capability for uptake Cu(II) and Pb(II) with a high regeneration properties as the introduction of the active site (–NH and $–NH_2$) while the process of membrane preparation was simplified in this way. Thence, the polyvinylidene fluoride and polyethyleneimine mixed membrane (PVDF-PEI) was used in this study.

Subsequently, a series of characterizations of PVDF-PEI were carried out. The adsorption and regeneration capability of PVDF-PEI were considered by batch experiments. In short, it reflects that PVDF-PEI has a good application prospect for uptake Cu(II) and Pb(II) from solution.

2. Materials and methods

2.1. Main reagents and instruments

All reagents were analytically pure and using water was deionized water. Formation in detail and all instrument used are listed in Table S1.

2.2. Preparation of materials

4.6 g PVDF (which had been vacuum dried for several hours at 60°C) was dissolved in 50 mL N,N-dimethylformamide and stirred in a magnetic stirring water bath under 60°C over 1 h; then took it out and added 10% (wt) PEI after cooling; then put it in a magnetic stirring water bath at 45°C over 3 h and put it overnight at room temperature, the casting solution could be acquired. The casting solution was coated with 1 mm thin layer in a Petri dish using a plastic dropper and dried in a vacuum oven for 0.5 h (60°C). Finally, elution, soaked and washed with water (for removing organic matter on the surface of PVDF-PEI), and PVDF-PEI blend film was obtained after air-dried and recorded as PVDF-PEI.

2.3. Characterization of materials

For understanding the property and mechanism of PVDF-PEI uptake Cu(II) and Pb(II), the same below). Firstly, Fourier-transform infrared spectroscopy (FTIR) analysis was used to identify whether PEI was successfully introduced. X-ray photoelectron spectroscopy (XPS) was utilized to examine the changes of the element on the surface of PVDF-PEI before and after adsorption.

2.4. Adsorption experiment

In the experiment, the performances of PVDF-PEI uptake Cu(II) and Pb(II) were considered through batch research, respectively. A certain amount of PVDF-PEI was put in several 50 mL conical flasks, and 20 mL Cu(II) or Pb(II) solution with a certain consistency of Cu(II) and Pb(II) was added. The mixtures were continuously shaken in a water bath under a constant temperature, 120 rpm, for some time, separately. The influences of the solution pH (2.0–5.5), PVDF-PEI quality (5–40 mg), salinity (0–0.20 mol L^{-1} $NaNO_3$ and KNO_3), contact time (0–8 h) and contact temperature (20°C, 30°C and 40°C) on the removing of Cu(II) and Pb(II) by PVDF-PEI were discussed, respectively. Among them, the solution pH were adjusted with NaOH and HCl or HNO_3 solution by using a pH meter, separately. The density of Cu(II) and Pb(II) after adsorption was measured by atomic absorption spectrophotometry at their maximum absorption wavelength of 324.7 and 283.3 nm, respectively.

The uptake capacity and removal rate were computed by Eqs. (1) and (2), separately.

$$q = \frac{V\left(C_0 - C\right)}{m} \tag{1}$$

$$p = \frac{\left(C_0 - C\right)}{C_0} \times 100\% \tag{2}$$

where q indicates the unit uptake capacity (mg g^{-1}); m denotes the mass of PVDF-PEI (g); V means the bulk of Cu(II) or Pb(II) solution (L); p indicates the removal efficiency (%); C_0 and C show the content of Cu(II) and Pb(II) before and after adsorption (mg L^{-1}), respectively.

2.5. Adsorption kinetics

PVDF-PEI (0.010 g) was added to multiple conical flasks containing 20 mL Cu(II) or Pb(II) solution of three

initial density, respectively. Then, put in a constant temperature water bath over 20°C, 30°C, 40°C with 120 rpm, separately. The q_t of Cu(II) and Pb(II) was obtained at different times (0–8 h).

2.6. Adsorption isotherm

Transferred 20 mL Cu(II) or Pb(II) solution under different initial consistency to multiple conical flasks. Further added 10 mg of PVDF-PEI, and put it in a water bath over 20°C, 30°C, 40°C, 120 rpm for 8 h, separately. Finally, the q_e was calculated.

2.7. Desorption regeneration

For judging the economic benefits of PVDF-PEI, this study explored the recycling performance of PVDF-PEI. First, weigh 10 mg PVDF-PEI in two conical flasks containing 20 mL of 250 mg L^{-1} Cu(II) or 200 mg L^{-1} Pb(II) solution, and put it in a water bath over 30°C, 120 rpm for 8 h, next took out PVDF-PEI, washed them three times with water and dried naturally. Then PVDF-PEI-Cu and PVDF-PEI-Pb were obtained and calculated the unit adsorption amount q_m. Then added 20 mL 0.1 mol L^{-1} HCl or HNO_3 to the conical flask with 10 mg PVDF-PEI-Cu or PVDF-PEI-Pb, separately; and desorbed for 8 h in a water bath over 30°C, 120 *r*; calculated the desorption rate (*d*). Finally, washed the desorbed adsorbent three times with water, and then reused them. Same operation as above and calculated the regeneration rate (*r*). Three desorption regenerations were performed.

The *d* and *r* are calculated by Eqs. (3) and (4), respectively.

$$d = \frac{m_d}{m_0} \times 100\% \tag{3}$$

$$r = \frac{q_r}{q_m} \times 100\% \tag{4}$$

where *d* notes the desorption efficiency, *r* means the regeneration efficiency, m_d represents the mass of PVDF-PEI after desorption, m_0 indicates the mass of the adsorbate on PVDF-PEI after adsorption, q_r expresses the unit adsorption amount when adsorbed again, and q_m shows the unit adsorption amount before desorption.

3. Results and discussion

3.1. Characterization

3.1.1. FTIR analysis

For knowing the changes of the functional groups on PVDF-PEI, as well as the form of action for Cu(II) and Pb(II) with PVDF-PEI, related materials are subjected by FTIR analysis (Fig. 1). As illustrated, the feature peaks at 840; 883; 1,070; 1,181; 1,275 and 1,400 cm^{-1} belonged to the raw PVDF, these peaks were formed by the rocking and stretching of the C–F, C–H and C–H bonds [20]. After PVDF and PEI blending, there were new peaks at 3,313 and 1,650 cm^{-1}, which could be seen as the stretching vibration and bending vibration of N–H in PEI [21,22], respectively; In addition, two peaks were both weakened after uptaking Cu(II) or Pb(II), which thanked for the formation of coordination bonds between Cu(II) or Pb(II) and N in PEI [19]. The above results indicated that PVDF and PEI were blended successfully, and Cu(II) and Pb(II) were adsorbed in a complex form.

3.1.2. XPS analysis

For further understanding the mode of action of Cu(II) as well as Pb(II) with PVDF-PEI, XPS analysis is carried out; and the high-resolution spectra of some elements is also performed (Fig. 2). It was clearly observed from Fig. 2a that there were some peaks at 284.66, 398.00, 530.29, and 686.46 eV of PVDF-PEI, which were attributed to C1s, N1s, O1s, and F1s, respectively. Two new peaks appeared at 932.76 eV of PVDF-PEI-Cu and 141.00 eV of PVDF-PEI-Pb, which were the peak of Cu2p and Pb4f, respectively. It indicated that Cu(II) and Pb(II) had been successfully adsorbed on PVDF-PEI. In addition, the peak of O1s for PVDF-PEI-Cu and PVDF-PEI-Pb was obviously enhanced, this was attributed to hydrated hydroxyl in the empty orbit of copper and lead with the coordination between Cu(II) or Pb(II) and –NH or $–NH_2$ in PVDF-PEI.

It was shown from Fig. 2b that two peaks at 399.6 and 401.99 eV from N1s on PVDF-PEI belonged to C–N and protonated C–N, separately [23]; and the corresponding peak areas were 82.36 and 17.64%, respectively. The positions of the two peaks were slightly shifted to 399.62 and 402.03 eV after uptake Cu(II), respectively; the peak area also changed, which was 77.41% and 22.59%, respectively. These changes could be seen as the conformation of $–NH_2Cu^{2+}$ by the interaction between Cu(II) and $–NH_2$ or $–NH_3^+$ in PVDF-PEI or the formation of –NH–Cu by the lone electron pair of N in PEI attacking the empty orbit of Cu, which resulted in a slight increase in the binding energy of C–N and an increase in the protonated C–N content [24]. After Cu2p was subjected to peak resolution (Fig. 2c), two peaks were obtained at 932.76 and 952.72 eV, corresponding to Cu2p3/2 and Cu2p1/2, respectively [25]. Moreover, after adsorption of Pb(II) (Fig. 2b), three peaks were obtained after peak separation of N1s, which were 398.37, 400.16

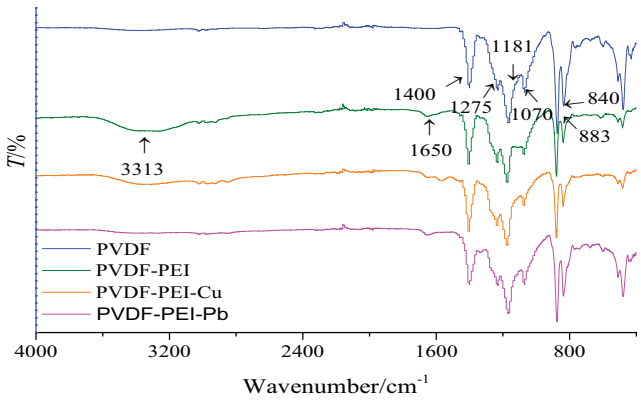

Fig. 1. FTIR of various materials.

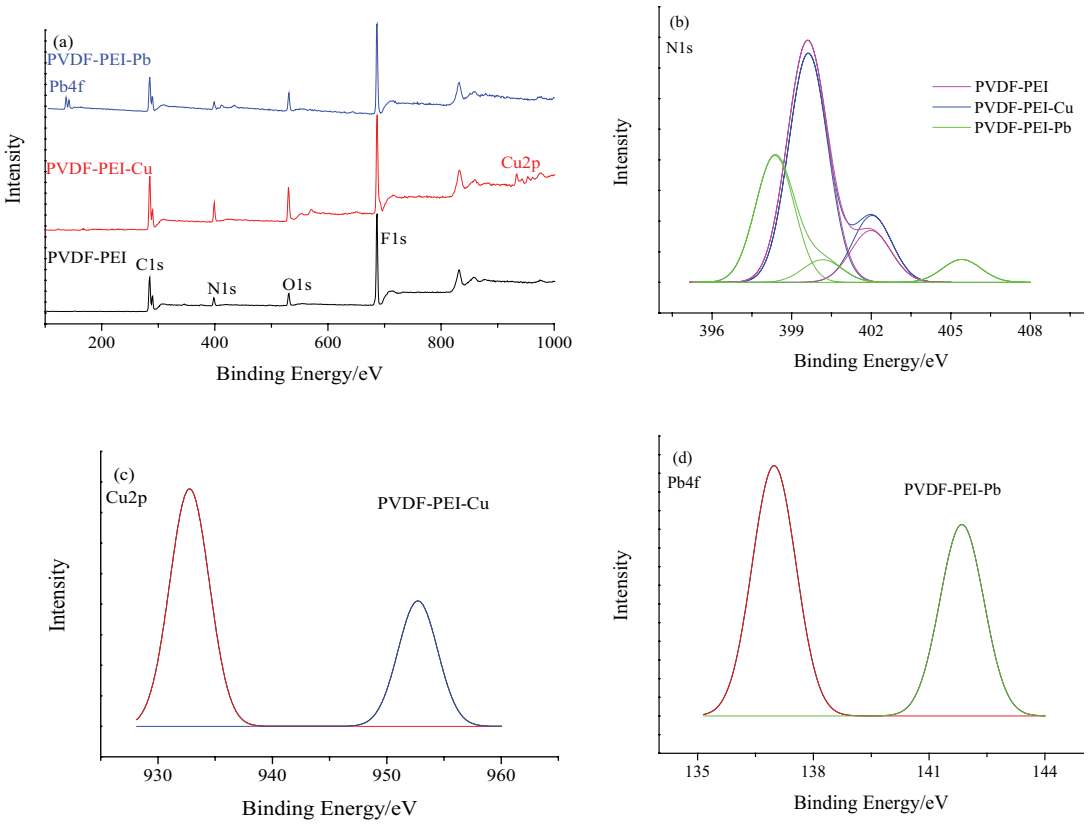

Fig. 2. XPS analysis of total energy spectrum (a) and high-resolution spectrum of N1s (b), Cu2p (c) and Pb4f (d).

and 405.41 eV, respectively corresponding to C–N, partially protonated C–N and –NH···Pb, the peak areas were 73.60%, 13.13% and 13.2%, separately. The peaks at 399.6 and 401.99 eV shifted left to 398.37 and 400.16 eV, respectively; and the peak areas decreased to 73.60% and 13.13%, respectively. This because of the formation of –NH–Pb by the lone electron pair on N in PEI assaulting the empty orbit of Pb or the formation of $–NH_2Pb^{2+}$ by the interaction of Pb with protonated C–N. As a result, the binding effect of N was increased, which reduced the binding energy and the corresponding peak area. Pb4f was split into two peaks at 136.98 and 141.85 eV (Fig. 2d), corresponding to Pb4f7/2 and Pb4f5/2 [26]. Compared with the peak separation of Pb in pure $PbNO_3$ (standard peak position Pb4f7/2: 139.6 eV; Pb4f5/2: 144.5 eV), there was a left shift phenomenon [27], this was because the lone pair of electrons on N of PEI occupy the empty orbits of Pb, causing the peak of Pb4f to move to a lower binding energy. Comprehensively showed that the process of PVDF-PEI uptake Cu(II) and Pb(II) is mainly based on complexation and ion exchange.

3.2. Adsorption studies

3.2.1. Batch adsorption studies

During the adsorption exploration, the solution pH, adsorbent dosage and system salinity are major indicators in evaluating the adsorption capacity of PVDF-PEI (Fig. 3). It was found from Fig. 3a that the adsorption capacity of Cu(II) and Pb(II) by PVDF-PEI enhanced as the solution pH increased, and the capacity of PVDF-PEI uptake Cu(II) finally decreased slightly. This was because the surface of PVDF-PEI showed a positive charge, and the electrostatic repulsion was large, and it is not easy to adsorb when the solution pH of Cu(II) and Pb(II) was lower than pH_{zpc} of PVDF-PEI (The isoelectric point of PVDF-PEI measured was 7.3 in this study) in the range of 2–5.5 [28]. However, the degree of deprotonation of PVDF-PEI increased, and the electrostatic repulsion decreased with the increase of solution pH during the range of 2–5.5 [29]. Meanwhile, it was easier for PVDF-PEI reacting with Cu(II) and Pb(II) combined with the competitive adsorption weakened between Cu(II) or Pb(II) and H_3O^+ as the acidity declined [30]. Furthermore, the progress of adsorption would be inhibited with the degree of deprotonation of Cu(II) and Pb(II) increased with the alkalinity rised. As the pH further increased, they would exist as $Cu(OH)_2$ and $Pb(OH)_2$, respectively [31]. Therefore, the adsorption performance of Cu(II) on PVDF-PEI decreased slightly finally. In addition, the maximum adsorption value at pH = 5.0 of Cu(II). The pH was not adjusted backwards for avoiding the precipitation of Pb(II). In this experiment, pH = 5.0 was used for Cu(II) adsorption while pH = 5.2 was selected for removing Pb(II), that was, the pH of the original solution. Existing literature points to similar results. For example, chitosan/polyvinyl alcohol beads functionalized with polyethylene glycol adsorb Cu(II) [32]; magnetic composite microgel uptakes Pb(II) [33]. All shows that the solution pH = 5 was beneficial for removing Cu(II) or Pb(II).

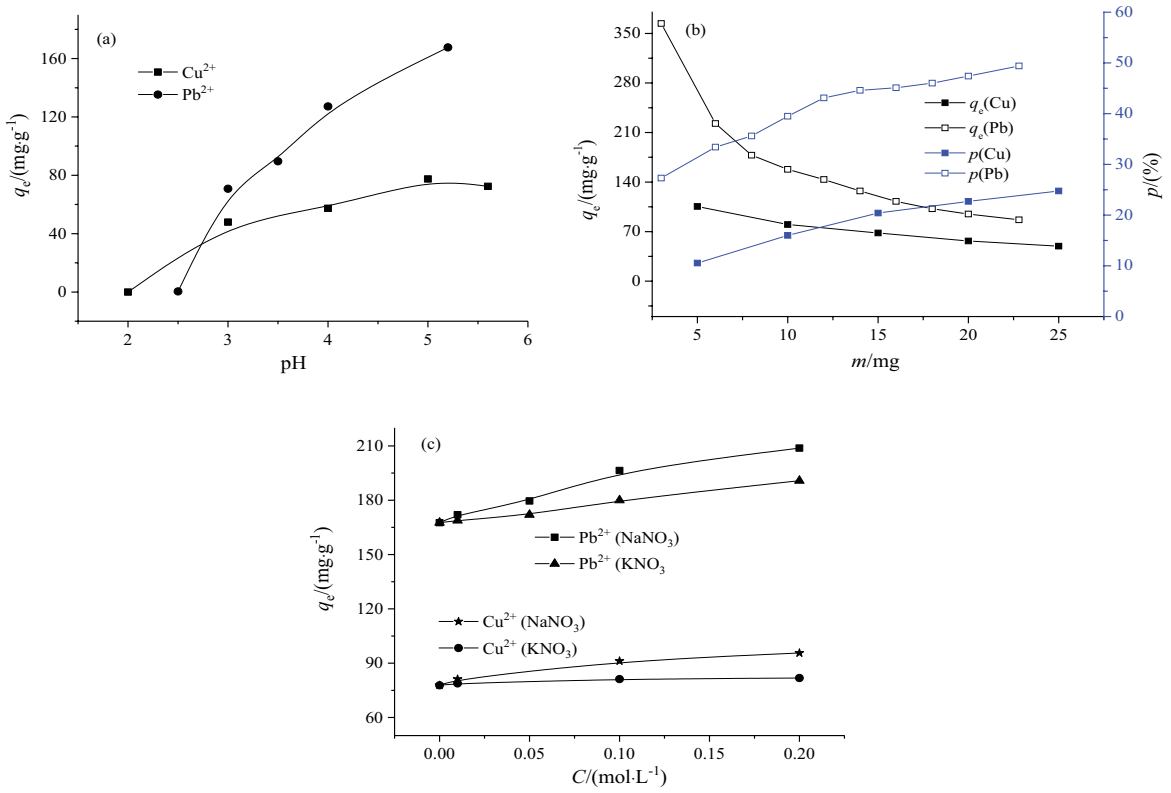

Fig. 3. Effect of pH (a), PVDF-PEI dosage (b) and salinity (c) on Cu(II) (C_0 = 250 mg L^{-1}) and Pb(II) (C_0 = 200 mg L^{-1}) adsorption.

It was clearly seen from Fig. 3b that the unit adsorption amount gradually decreased but the removal rate suddenly raised of Cu(II) and Pb(II) with the mass of PVDF-PEI increased. This was because the relatively bound Cu(II) and Pb(II) gently reduced as the mass of PVDF-PEI increased when the amount of Cu(II) and Pb(II) was constant, so the adsorption amount thinly decreased. However, due to the active site on PVDF-PEI was limited, the removal rate slowly increased with the active site increased gradually as the mass of PVDF-PEI increased. Considering the utilization rate of PVDF-PEI and removal rate of pollution, 10 mg as the mass of PVDF-PEI was selected for subsequent experiments.

It was noticed from Fig. 3c that the presence of Na^+ and K^+ were both favorable for removing Cu(II) and Pb(II), and the effect of Na^+ was slightly larger than K^+ (possibly due to the smaller ionic radius of Na^+ than K^+). However, the effect of salinity was weak on the whole, so it could be neglected in subsequent experiments. Similar results are common in existing studies. For example, polyethyleneimine-modified wheat straw [34] is less affected by salinity. Fe_3O_4@DAPF has a good selectivity for Pb(II) with a little affected by coexisting ions [28]. It was shown that PVDF-PEI had good selectivity for Cu(II) and Pb(II) with a certain salt tolerance. So the action of salinity can be neglected in subsequent research.

3.2.2. Adsorption kinetics

For investigating the mechanism of Cu(II) and Pb(II) by PVDF-PEI, the kinetics of adsorption are carried out (Figs. 4 and S1). It was evidently found from Figs. 4 and S1 that the unit adsorption amount of Cu(II) and Pb(II) raised rapidly and finally tended to balance by PVDF-PEI as the adsorption proceeding. The reason for the point could be interpreted as the number of active sites on PVDF-PEI kept decreasing as the adsorption progressing, resulted in a decrease in the relatively binding active sites of PVDF-PEI, then the adsorption proceeded slowly and the adsorption tended to be balanced.

For judging the mechanism and speed control step of the adsorption process, the three kinetic models (pseudo-first-order model, pseudo-second-order model, Elovich equation listed in Table S2) were chosen to nonlinearly fit the adsorption kinetics curve. The fitting parameters are shown in Tables S3 and S4, respectively while the fitted curves are also shown in Figs. 4 and S1.

As shown in Tables S3 and S4, compared with pseudo-second-order model, the theoretical and experimental adsorption amount were closer as the process of uptaking Cu(II) and Pb(II) pictured by pseudo-first-order model; In addition, there were larger $R^2 \geq 0.974$ and smaller SSE ≤ 115 of Cu(II), and larger $R^2 \geq 0.915$ and smaller SSE ≤ 770 of Pb(II). Therefore, pseudo-first-order model was better for fitting these two processes and revealed that there was physical adsorption. It has been shown in the existing research that pseudo-first-order model can better bewrite the adsorption process of Cu(II) and Pb(II) compared with pseudo-second-order model. The Elovich model had a large R^2 and a small SSE, and also be well to fit these two adsorption processes; It demonstrated that there were heterogeneous chemisorption and ion exchange in these two

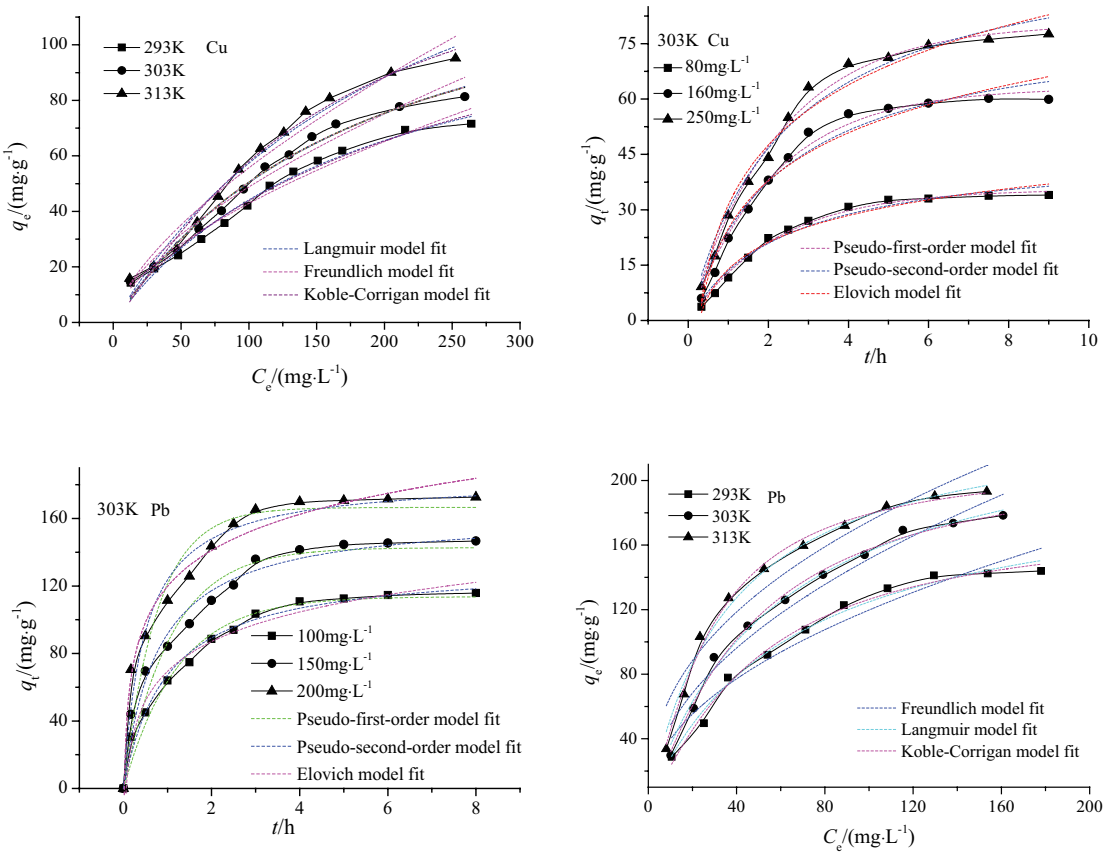

Fig. 4. Adsorption kinetics (303 K) and isotherm of Cu(II) and Pb(II) adsorption on PVDF-PEI.

adsorption processes. In summary, it was shown that these two adsorption processes were a complicated process: physical adsorption and chemical adsorption coexist.

3.2.3. Adsorption isotherm study

For further understanding the adsorption mechanism and the feasibility in practical application of the process of PVDF-PEI uptake Cu(II) and Pb(II), the isothermal adsorption studies are carried out. It was seen from Fig. 4 that the unit adsorption amount of Cu(II) and Pb(II) increased first, then tended to balance by PVDF-PEI with the equilibrium concentration increased, respectively. It was due to the active sites on PVDF-PEI could bind more adsorbate with the content of Cu(II) and Pb(II) increased. Therefore, values of q_e increased drastically in the early stage. However, as the active sites on PVDF-PEI was limited, values of q_e about Cu(II) and Pb(II) no longer increased while tended to balance as the content of Cu(II) and Pb(II) increased to a certain extent.

To determine the reaction form as well as the theoretical adsorption capacity, the adsorption isotherms are nonlinearly fitted using the following several isothermal models for comparison (fitted curves shown in Fig. 5). The corresponding forms of models are displayed in Table S2, and the fitting parameters are listed in Tables 1 and 2, respectively.

It was evidently observed from Tables 1 and 2 that Langmuir model had a larger R^2 and a smaller SSE, but $q_{e(\text{theo})}$ and $q_{e(\text{exp})}$ had a large difference. Therefore, the adsorption process cannot be simply regarded as a single-layer uniform adsorption.

For Freundlich model, values of $1/n$ (0.604–0.664 for Cu, 0.423–0.495 for Pb) demonstrated that the process of PVDF-PEI uptaking Cu(II) and Pb(II) were easy to carry out. In addition, there were large R^2 and small SSE, reflected that Freundlich model could better fit these two adsorption processes, which indicated that there was non-uniform surface adsorption during these two adsorption processes.

Koble–Corrigan model had a large R^2 and a small SSE. In addition, the value of B and n tended to 0 and 1, respectively; which could be converted into the Langmuir model and further demonstrated that these two adsorption process contained uniform surface adsorption.

In summary, it demonstrated that these two adsorption processes were a complex process: non-uniform surface multi-layer adsorption and uniform surface monolayer adsorption coexist. Han et al. showed that Freundlich and Langmuir could describe the process of citric acid-modified wheat straw for removal of copper ion and methylene blue [35]. Ma et al. pointed out that Langmuir model showed a good correlation for the description of xanthate-modified wheat straw uptaking copper ion [36]. These all reflect the complexity of heavy metal ions adsorption.

PVDF-PEI has a better adsorption performance for Cu(II) and Pb(II) compared with general adsorbents (Table S5). So, it can be considered to removal Cu(II) and Pb(II) from water.

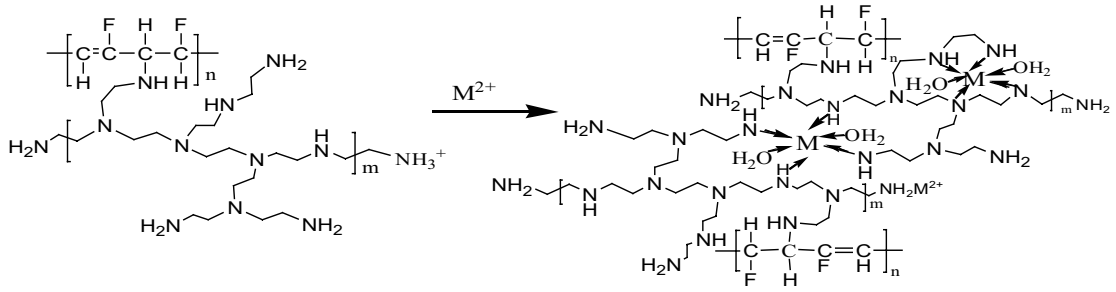

Fig. 5. Adsorption mechanism of M(II) (M means Cu and Pb).

Table 1
Adsorption isotherm fitting parameters of Cu(II)

Langmuir					
T (K)	$q_{m(exp)}$ (mg g^{-1})	K_L (L mg^{-1})	$q_{m(theo)}$ (mg g^{-1})	R^2	SSE
293	71.5	5.32E-3 ± 8.43E-4	127 ± 11	0.979	80.9
303	81.3	5.08E-3 ± 8.06E-4	149 ± 14	0.980	101
313	95.2	4.28E-3 ± 7.25E-4	191 ± 20	0.982	135
Freundlich					
T (K)	$q_{m(exp)}$ (mg g^{-1})	K_F	$1/n$	R^2	SSE
293	71.5	2.65 ± 0.50	0.604 ± 0.037	0.973	102
303	81.3	2.78 ± 0.60	0.622 ± 0.045	0.967	172
313	95.2	2.61 ± 0.60	0.664 ± 0.045	0.967	241
Koble–Corrigan					
T (K)	A	B	n	R^2	SSE
293	1.06 ± 0.63	6.71E-3 ± 1.89E-3	0.878 ± 0.163	0.978	76.7
303	0.637 ± 0.424	4.54E-3 ± 2.11E-3	1.05 ± 0.18	0.978	101
313	0.423 ± 0.295	2.78E-3 ± 1.48E-3	1.17 ± 0.18	0.981	124

3.2.4. Thermodynamic study

In practice, the feasibility of the adsorption reaction can be inferred by ΔG, ΔH, and ΔS, which calculates from Eqs. (5)–(8) [37,38].

$$K_c' = \frac{C_{ad,e}}{C_e} \tag{5}$$

$$\Delta G = -RT\ln K_c' \tag{6}$$

$$\Delta G = \Delta H - T\Delta S \tag{7}$$

$$\ln k = -\frac{E_a}{RT} + \ln A \tag{8}$$

where $C_{ad,e}$ and C_e are the concentrations of Cu(II) and Pb(II) on PVDF-PEI and in the solution when the adsorption get balance; ΔG represents the Gibbs free energy (J); R means the gas constant (8.314 J mol^{-1} K^{-1}); T represents the absolute temperature (K); K_c' shows the adsorption equilibrium constant; k indicates the adsorption rate constant, E_a shows the apparent activation energy (kJ mol^{-1}), and A shows the temperature influence factor.

Through related calculations, the thermodynamic parameters of PVDF-PEI uptaking Cu(II) and Pb(II) was calculated (Table 3).

It was obviously noticed from Table 3 that the negative ΔG decreased with the temperature increased, indicated that the process of PVDF-PEI uptaking Cu(II) and Pb(II) was spontaneous with the spontaneous enhancement as the temperature increased. Positive ΔH revealed that these two reactions were endothermic. Positive ΔS reflected that the disorder increased as Cu(II) and Pb(II) shifted from the solvent phase to PVDF-PEI surface during the adsorption process [10]. E_a is often used to judge the type of adsorption. Positive E_a showed that these two adsorption processes were endothermic. In addition, $\Delta H \neq$ 40–120 kJ mol^{-1}, and $E_a \neq$ 5–40 kJ mol^{-1}, indicated that these two processes could be seen as physicochemical adsorption [40,41]. In summary, the adsorption process of Cu(II) and Pb(II) on PVDF-PEI were both endothermic reactions with spontaneous and entropy increased with physical adsorption and chemical adsorption.

Table 2
Adsorption isotherm fitting parameters of Pb(II)

Langmuir					
T (K)	$q_{e(exp)}$ (mg g^{-1})	K_L (L mg^{-1})	$q_{m(theo)}$ (mg g^{-1})	R^2	SSE
293	144	1.57E-2 ± 0.18E-2	204 ± 9	0.986	188
303	178	1.70E-2 ± 0.15E-2	248 ± 9	0.992	169
313	193	2.73E-2 ± 0.26E-2	244 ± 8	0.988	286
Freundlich					
T (K)	$q_{e(exp)}$ (mg g^{-1})	K_F	1/n	R^2	SSE
293	144	13.1 ± 3.0	0.480 ± 0.049	0.942	97.1
303	178	15.5 ± 3.2	0.495 ± 0.045	0.955	116
313	193	24.9 ± 5.4	0.423 ± 0.048	0.928	214
Koble–Corrigan					
T (K)	A	B	n	R^2	SSE
293	1.59 ± 0.79	8.92E-3 ± 3.87E-3	1.22 ± 0.15	0.988	141
303	2.43 ± 0.85	1.11E-2 ± 0.33E-2	1.18 ± 0.11	0.993	120
313	2.95 ± 0.95	1.38E-2 ± 0.40E-2	1.29 ± 0.11	0.993	137

Table 3
Thermodynamic parameters of Cu(II) and Pb(II)

Adsorbate	E_a (kJ mol^{-1})	ΔH (kJ mol^{-1})	ΔS (J mol^{-1} K^{-1})	ΔG (kJ mol^{-1})		
				293 K	303 K	313 K
Cu(II)	2.76	24.7	85.7	–0.489	–1.02	–2.20
Pb(II)	4.51	16.1	57.0	–0.745	–0.96	–1.88

3.2.5. Desorption regeneration

For exploring the economic benefits of adsorption process and recovery of valuable materials, it is essential to regenerate spent or adsorbate-loaded adsorbents [39–42]. The regenerative study is carried out for Cu or Pb loaded PVDF-PEI (Fig. S2).

As seen in Fig. S2, the desorption efficiency (d > 90%) and the regeneration efficiency (r > 90%) were basically unchanged during multiple desorption regenerations of Cu-loaded PVDF-PEI eluted with 0.1 mol L^{-1} HCl. The desorption rate and regeneration decreased slightly, but both were above 80% of Pb-loaded PVDF-PEI desorbed with 0.1 mol L^{-1} HNO_3. It declared that PVDF-PEI had a good regeneration performance.

3.2.6. Adsorption mechanism

Inferred adsorption mechanism can understand the adsorption process of Cu(II) and Pb(II) on PVDF-PEI, theoretically. From the FTIR analysis results, it was known that the N–H stretching and bending vibration at 3,313 and 1,650 cm^{-1} got weakened, respectively; it was because of the coordination of Cu(II) and Pb(II) with N in PEI. In XPS analysis, the peak of O1s indicated that the increase of the O–H binding energy peak area could thanks for the coordination of Cu(II) and Pb(II) with the N in PEI, and there were hydroxyl groups in the empty orbit of copper and lead. In addition, the increase of protonated C–N content of N 1s was due to the formation of $-NH_2Cu^{2+}$ and $-NH_2Pb^{2+}$ between Cu(II) or Pb(II) and $-NH_2$ or $-NH_3^+$ in PVDF-PEI. On the whole, it was concluded that these two adsorption processes be based on complex coordination and ion exchange (Fig. 5).

4. Conclusion

PVDF-PEI blend film had good adsorption properties for Cu(II) and Pb(II) with higher salt tolerance and regeneration. The isotherm fitting results showed that these two adsorption processes contained non-uniform surface multilayer adsorption and uniform surface monolayer adsorption. The kinetic fitting results declared that there was physicochemical adsorption during these two adsorption processes. The thermodynamic parameters indicated that both adsorption processes were the reaction of spontaneous and endothermic with entropy increased. In summary, PVDF-PEI has the potential to effectively eliminate Cu(II) or Pb(II) from solution.

Acknowledgement

This work was supported in part by the Key Scientific Research Project in Universities of Henan Province (19A150048).

References

[1] S. Afroze, T.K. Sen, A review on heavy metal ions and dye adsorption from water by agricultural solid waste adsorbents, Water Air Soil Pollut., 229 (2018) 225, doi: 10.1007/s11270-018-3869-z.

[2] H.Q. Qin, T.J. Hu, Y.B. Zhai, N.J. Lu, Aliyeva, The improved methods of heavy metals removal by biosorbents: a review, Environ. Pollut., 258 (2020) 113777, doi: 10.1016/j.envpol.2019.113777.

[3] S. Begum, N.Y. Yuhana, N.M. Saleh, N.H.N. Kamarudin, A.B. Sulong, Review of chitosan composite as a heavy metal adsorbent: material preparation and properties, Carbohydr. Polym., 259 (2021) 117613, doi: 10.1016/j.carbpol.2021.117613.

[4] W.S. Chai, J.Y. Cheun, P.S. Kumar, M. Mubashir, Z. Majeed, F. Banat, S.-H. Ho, P.L. Show, A review on conventional and novel materials towards heavy metal adsorption in wastewater treatment application, J. Cleaner Prod., 296 (2021) 126589, doi: 10.1016/j.jclepro.2021.126589.

[5] C.F. Carolin, P.S. Kumar, A. Saravanan, G.J. Joshiba, Mu. Naushad, Efficient techniques for the removal of toxic heavy metals from aquatic environment: a review, J. Environ. Chem. Eng., 5 (2017) 2782–2799.

[6] F.M. Mpatani, R.P. Han, A.A. Aryee, A.N. Kani, Z.H. Li, L.B. Qu, Adsorption performance of modified agricultural waste materials for removal of emerging micro-contaminant bisphenol A: a comprehensive review, Sci. Total Environ., 780 (2021) 146629, doi: 10.1016/j.scitotenv.2021.146629.

[7] F.M. Mpatani, A.A. Aryee, A.N. Kani, R.P. Han, Z.H. Li, E. Dovi, L.B. Qu, A review of treatment techniques applied for selective removal of emerging pollutant-trimethoprim from aqueous systems, J. Cleaner Prod., 308 (2021) 127359, doi: 10.1016/j.jclepro.2021.127359.

[8] H. Demiral, C. Güngör, Adsorption of copper(II) from aqueous solutions on activated carbon prepared from grape bagasse, J. Cleaner Prod., 124 (2016) 103–113.

[9] J.S. He, J.P. Chen, Cu(II)-imprinted poly(vinyl alcohol)/ply(acrylic acid) membrane for greater enhancement in sequestration of copper ion in the presence of competitive heavy metal ions: material development, process demonstration, and study of mechanisms, Ind. Eng. Chem. Res., 53 (2014) 20223–20233.

[10] Z. Li, D. Xiao, Y. Ge, S. Koehler, Surface-functionalized porous lignin for fast and efficient lead removal from aqueous solution, ACS Appl. Mater. Interfaces, 7 (2015) 15000–15009.

[11] R.M. Novais, L.H. Buruberri, M.P. Seabra, J.A. Labrincha, Novel porous fly-ash containing geopolymer monoliths for lead adsorption from wastewaters, J. Hazard. Mater., 318 (2016) 631–640.

[12] C. Jin, X.Y. Zhang, J.N. Xin, G.F. Liu, J. Chen, G.M. Wu, T. Liu, J.W. Zhang, Z.W. Kong, Thiol–Ene synthesis of cysteine-functionalized lignin for the enhanced adsorption of Cu(II) and Pb(II), Ind. Eng. Chem. Res., 57 (2018) 7872–7880.

[13] A.M. Nasir, P.S. Goh, M.S. Abdullah, B.C. Ng, A.F. Ismail, Adsorptive nanocomposite membranes for heavy metal remediation: recent progresses and challenges, Chemosphere, 232 (2019) 96–112.

[14] A. Simaite, B. Tondu, P. Soueres, C. Bergaud, Hybrid PVDF/PVDF-graft-PEGMA membranes for improved interface strength and lifetime of PEDOT: PSS/PVDF/ionic liquid actuators, ACS Appl. Mater. Interfaces, 7 (2015) 19966–19977.

[15] M.M. Tao, F. Liu, L.X. Xue, Hydrophilic poly(vinylidene fluoride) (PVDF) membrane by *in situ* polymerisation of 2-hydroxyethyl methacrylate (HEMA) and micro-phase separation, J. Mater. Chem., 22 (2012) 9131–9137.

[16] L. Song, F.Q. Liu, C.Q. Zhu, A.M. Li, Facile one-step fabrication of carboxymethyl cellulose based hydrogel for highly efficient removal of Cr(VI) under mild acidic condition, Chem. Eng. J., 369 (2019) 641–651.

[17] Z. Fan, K.H.L. Po, K.K. Wong, S. Chen, S.P. Lau, Polyethylenimine-modified graphene oxide as a novel antibacterial agent and its synergistic effect with daptomycin for methicillin-resistant *Staphylococcus aureus*, ACS Appl. Nano Mater., 1 (2018) 1811–1818.

[18] A.N. Kani, E. Dovi, A.A. Aryee, F.M. Mpatani, R.P. Han., Z.H. Li, L.B. Qu, Polyethyleneimine modified Tiger nut residue for removal of Congo red from solution, Desal. Water Treat., 215 (2021) 209–221.

[19] Y.Z. Wang, Y.Z. Chen, C.H. Wang, J. Sun, Z.P. Zhao, W.F. Liu, Polyethylenimine-modified membranes for CO_2 capture and in situ hydrogenation, ACS Appl. Mater. Interface, 10 (2018) 29003–29009.

[20] P. Biswas, N.A. Hoque, P. Thakur, M.M. Saikh, S. Roy, F. Khatun, B. Bagchi, S. Das, Highly efficient and durable piezoelectric nanogenerator and photo-power cell based on CTAB modified montmorillonite incorporated PVDF film, ACS Sustainable Chem. Eng., 7 (2019) 4801–4813.

[21] A. Jana, O. Roy, S.S. Ravuru, S. De, Tuning of graphene oxide intercalation in magnesium aluminium layered double hydroxide and their immobilization in polyacrylonitrile beads by single step mussel inspired phase inversion: a super adsorbent for lead, Chem. Eng. J., 391 (2020) 123587, doi: 10.1016/j.cej.2019.123587.

[22] X.Y. Xie, R.K. Deng, Y.Q. Pang, Y. Bai, W.J. Zheng, Y.H. Zhou, Adsorption of copper(II) by sulfur microparticles, Chem. Eng. J., 314 (2017) 434–442.

[23] X. Tang, Y. Zhou, M. Peng, Green preparation of epoxy/graphene oxide nanocomposites using a glycidylamine epoxy resin as the surface modifier and phase transfer agent of graphene oxide, ACS Appl. Mater. Interfaces, 8 (2016) 1854–1866.

[24] Y.L. Liu, J. Xu, Z. Cao, R.Q. Fu, C.C. Zhou, Z.N. Wang, X.H. Xu, Adsorption behavior and mechanism of Pb(II) and complex Cu(II) species by biowaste-derived char with amino functionalization, J. Colloid Interface Sci., 559 (2020) 215–225.

[25] Y. Wang, J. Im, J.W. Soares, D.M. Steeves, J.E. Whitten, Thiol adsorption on and reduction of copper oxide particles and surfaces, Langmuir, 32 (2016) 3848–3857.

[26] M. Hua, Y. Jiang, B. Wu, B. Pan, X. Zhao, Q. Zhang, Fabrication of a new hydrous Zr(IV) oxide-based nanocomposite for enhanced Pb(II) and Cd(II) removal from waters, ACS Appl. Mater. Interfaces, 5 (2013) 12135–12142.

[27] C.X. Yu, X. Han, Z.C. Shao, L.L. Liu, H.W. Hou, High efficiency and fast removal of trace Pb(II) from aqueous solution by carbomethoxy-functionalized metal–organic framework, Cryst. Growth Des., 18 (2018) 1474–1482.

[28] S. Venkateswarlu, M. Yoon, Core-shell ferromagnetic nanorod based on amine polymer composite (Fe_3O_4@DAPF) for fast removal of Pb(II) from aqueous solutions, ACS Appl. Mater. Interfaces, 7 (2015) 25362–25372.

[29] X. Li, J.L. Xing, C.L. Zhang, B. Han, Y.H. Zhang, T. Wen, R. Leng, Z.H. Jiang, Y.J. Ai, X.K. Wang, Adsorption of lead on sulfur-doped graphitic carbon nitride nanosheets: experimental and theoretical calculation study, ACS Sustainable Chem. Eng., 6 (2018) 10606–10615.

[30] A.B. Dichiara, M.R. Webber, W.R. Gorman, R.E. Rogers, Removal of copper ions from aqueous solutions via adsorption on carbon nanocomposites, ACS Appl. Mater. Interfaces, 7 (2015) 15674–15680.

[31] A.M. Yousif, O.F. Zaid, W.A. El-Said, E.A. Elshehy, I.A. Ibrahim, Silica nanospheres-coated nanofibrillated cellulose for removal and detection of copper(II) ions in aqueous solutions, Ind. Eng. Chem. Res., 58 (2019) 4828–4837.

[32] D.G. Trikkaliotis, A.K. Christoforidis, A.C. Mitropoulos, G.Z. Kyzas, Adsorption of copper ions onto chitosan/poly(vinyl alcohol) beads functionalized with poly(ethylene glycol), Carbohyd. Polym., 234 (2020) 115890, doi: 10.1016/j.carbpol.2020.115890.

[33] L.P. Jiang, P. Liu, Novel magnetic fly ash/poly(acrylic acid) composite microgel for selective adsorption of Pb(II) ion: synthesis and evaluation, Ind. Eng. Chem. Res., 53 (2014) 2924–2931.

[34] J.J. Dong, Y.Y. Du, R.S. Duyu, Y. Shang, S.S. Zhang, R.P. Han, Adsorption of copper ion from solution by polyethylenemine modified wheat straw, Bioresour. Technol. Rep., 6 (2019) 96–102.

[35] R.P. Han, L.J. Zhang, C. Song, M,M. Zhang, H.M. Zhu, L.J. Zhang, Characterization of modified wheat straw, kinetic and equilibrium study about copper ion and methylene blue adsorption in batch mode, Carbohydr. Polym., 79 (2010) 1140–1149.
[36] Q.H. Guo, Z.Y. Zang, J. Ma, J.Y. Li, T. Zhou, R.P. Han, Adsorption of copper ions from solution using xanthate wheat straw, Water Sci. Technol., 82 (2020) 2029–2038.
[37] C.H. Ma, X.T. Zhang, K. Wen, R. Wang, R.P. Han, Facile synthesis of polyethyleneimine@Fe_3O_4 loaded with zirconium for enhanced phosphate adsorption: performance and adsorption mechanism, Korean J. Chem. Eng., 38 (2021) 135–143.
[38] J.L. Wang, X. Liu, M.M. Yang, H.Y. Han, S.S. Zhang, G.F. Ouyang, R.P. Han, Removal of tetracycline using modified wheat straw from solution in batch and column modes, J. Mol. Liq., 338 (2021) 116698.
[39] N.I. Taib, N.A. Rosli, N.I. Saharrudin, N.M. Rozi, N.A.A. Kasdiehram, N.N.T. Abu Nazri, Kinetic, equilibrium, and thermodynamic studies of untreated watermelon peels for removal of copper(II) from aqueous solution, Desal. Water Treat., 227 (2021) 289–299.
[40] H.N. Bhatti, Z. Mahmood, A. Kausar, S.M. Yakout, O.H. Shair, M. Iqbal, Biocomposites of polypyrrole, polyaniline and sodium alginate with cellulosic biomass: adsorption–desorption, kinetics and thermodynamic studies for the removal of 2,4-dichlorophenol, Int. J. Biol. Macromol., 153 (2020) 146–157.
[41] B.L. Zhao, W. Xiao, Y. Shang, H.M. Zhu, R.P. Han, Adsorption of light green anionic dye using cationic surfactant-modified peanut husk in batch mode, Arab. J. Chem., 10 (2017) S3595–S3602.
[42] A.A. Aryee, E. Dovi, X.X. Shi, R.P. Han, Z.H. Li, L.B. Qu, Zirconium and iminodiacetic modified magnetic peanut husk as a novel adsorbent for the sequestration of phosphates from solution: characterization, equilibrium and kinetic study, Colloid. Surf. A, 615 (2021) 126260, doi: 10.1016/j.colsurfa.2021.126260.

Supplementary information

Table S1
Main reagents and instruments

Instrument or Reagent Name	Related information
Polyvinylidene fluoride (PVDF)	Zhengzhou Zhongyuan District Innovation Laboratory Equipment Business Department, (China)
N,N-Dimethylformamide (DMF)	Fuchen Chemical Reagent Co., Ltd., (China)
Polyethyleneimine (PEI)	Shanghai Aladdin Biochemical Technology Co., Ltd., (China)
Anhydrous copper sulfate ($CuSO_4$)	Tianjin Damao Chemical Reagent Factory, (China)
Lead nitrate ($Pb(NO)_2$)	Tianjin Kemiou Chemical Reagent Co., Ltd., (China)
Precision acidity meter	PHS-3C Shanghai Instrument Electric Scientific Instrument, (China)
Constant temperature oscillator	SHZ-82 Changzhou Guohua Electric Co., Ltd., (China)
Electric blast drying oven	DHG-9055A Shanghai Yiheng Scientific Instrument, (China)
Atomic absorption spectrophotometer	AA-7020 Beijing East West Analysis Instrument Co., Ltd., (China)
Magnetic stirring water bath	EMS-20 Changzhou Renhe Instrument Factory, (China)
Fourier-transform infrared spectroscopy	PE-1710FTIR American PE Company
X-ray photoelectric energy spectrum	XPS ESCALAB 250Xi, Thermo Fisher, UK

Table S2
Several common adsorption models

Models	Nonlinear form	Symbol description
Isotherm model		
Langmuir	$q_e = \frac{q_m K_L C_e}{1 + K_L C_e}$	Describes a single layer uniform adsorption process in a rational state: q_m (mg g^{-1}) is monolayer theoretical saturated adsorption amount at equilibrium; K_L (L mg^{-1}) represents the Langmuir model constant associated with adsorption energy.
Freundlich	$q_e = K_F C_e^{1/n}$	Depicts multilayer and heterogeneous adsorption processes in non-ideal states: K_F and $1/n$ mean the Freundlich model constants related to adsorption capacity and adsorption intensity, respectively.
Koble–Corrigan	$q_e = \frac{AC_e^n}{1 + BC_e^n}$	Combination of the Langmuir and Freundlich model as a three-parameter model: A, B, n are model parameters.
Kinetic model		
Pseudo-first-order	$q_t = q_e\left(1 - e^{-k_1 t}\right)$	Describes the adsorption process of physical speed control: q_t (mg g^{-1}) is the unit adsorption amount of PVDF-PEI at time t; k_1 represents the pseudo-first-order kinetic model rate constant.
Pseudo-second-order	$q_t = \frac{k_2 q_e^2 t}{1 + K_2 q_e t}$	Depicts the chemically controlled adsorption process: k_2 indicates the pseudo-second-order kinetic model rate constant.
Elovich	$q_t = A + B\ln t$	Notes heterogeneous diffusion processes: A, B signifies constants.

Table S3
Adsorption kinetics fitting parameters of Cu(II)

Pseudo-first-order						
T (K)	C_0 (mg L^{-1})	$q_{e(\exp)}$ (mg g^{-1})	$q_{e(\text{theo})}$ (mg g^{-1})	k_1 (h^{-1})	R^2	SSE
293	250	71.3	75.2 ± 2.5	0.439 ± 0.039	0.979	115
	160	54.0	56.5 ± 2.1	0.444 ± 0.044	0.974	82.9
	80	33.2	36.4 ± 1.4	0.347 ± 0.031	0.983	22.1
303	250	77.6	80.4 ± 1.7	0.441 ± 0.025	0.991	55.0
	160	59.9	63.1 ± 1.6	0.464 ± 0.031	0.986	54.4
	80	34.0	35.6 ± 0.8	0.452 ± 0.027	0.990	12.2
313	250	90.0	92.6 ± 1.6	0.469 ± 0.022	0.993	51.5
	160	68.6	70.7 ± 1.2	0.425 ± 0.019	0.994	25.9
	80	36	36.4 ± 0.4	0.513 ± 0.017	0.996	4.34
Pseudo-second-order						
T (K)	C_0 (mg L^{-1})	$q_{e(\exp)}$ (mg g^{-1})	$q_{e(\text{theo})}$ (mg g^{-1})	k_2 (g mg^{-1} h^{-1})	R^2	SSE
293	250	71.3	98.6 ± 7.2	3.97E-3 ± 1.02E-3	0.958	229
	160	54.0	74.1 ± 5.8	5.32E-3 ± 1.47E-3	0.952	153
	80	33.2	50.0 ± 4.0	5.68E-3 ± 1.45E-3	0.969	39.4
303	250	77.6	105 ± 5	3.85E-3 ± 7.13E-4	0.976	139
	160	59.9	81.6 ± 5.1	5.24E-3 ± 1.18E-3	0.965	133
	80	34	46.2 ± 2.6	8.97E-3 ± 1.81E-3	0.972	33.2
313	250	90.0	119 ± 6	3.72E-3 ± 6.26E-4	0.978	163
	160	68.6	92.6 ± 4.4	4.14E-3 ± 6.92E-4	0.981	84.2
	80	36.0	45.8 ± 1.6	1.11E-2 ± 1.44E-3	0.985	16.3
Elovich						
T (K)	C_0 (mg L^{-1})	$q_{e(\exp)}$ (mg g^{-1})	A	B	R^2	SSE
293	250	71.3	28.2 ± 1.9	22.7 ± 1.4	0.957	237
	160	54.0	21.0 ± 1.5	17.3 ± 1.1	0.955	144
	80	33.2	11.5 ± 0.8	10.9 ± 0.6	0.967	42.0
303	250	77.6	31.3 ± 1.7	23.5 ± 1.26	0.969	179
	160	59.9	24.8 ± 1.5	18.8 ± 1.1	0.961	146
	80	34.0	13.9 ± 0.8	10.5 ± 0.6	0.967	38.4
313	250	90.0	38.0 ± 1.9	26.6 ± 1.5	0.967	245
	160	68.6	26.9 ± 1.4	20.6 ± 1.0	0.973	120
	80	36.0	15.9 ± 0.6	10.2 ± 0.5	0.975	27.4

Note: SSE = $\sum\left(q-q_c\right)^2$, q and q_c are values of adsorption quantity from the experiments and calculation according the model, respectively.

Table S4
Adsorption kinetics fitting parameters of Pb(II)

Pseudo-first-order						
T (K)	C_0 (mg L^{-1})	$q_{e(exp)}$ (mg g^{-1})	$q_{e(theo)}$ (mg g^{-1})	k_1 (h^{-1})	R^2	SSE
293	100	93.2	94.0 ± 1.4	0.779 ± 0.038	0.994	59.2
	150	126	128 ± 3	0.685 ± 0.052	0.987	248
	200	143	142 ± 4	0.867 ± 0.098	0.968	713
303	100	116	114 ± 3	0.817 ± 0.084	0.974	373
	150	147	143 ± 5	0.930 ± 0.130	0.949	102
	200	173	167 ± 6	1.30 ± 0.22	0.925	128
313	100	131	133 ± 3	0.877 ± 0.067	0.979	420
	150	167	165 ± 5	0.898 ± 0.091	0.975	770
	200	189	183 ± 8	1.12 ± 0.20	0.915	289
Pseudo-second-order						
T (K)	C_0 (mg L^{-1})	$q_{e(exp)}$ (mg g^{-1})	$q_{e(theo)}$ (mg g^{-1})	k_2 (g mg^{-1} h^{-1})	R^2	SSE
293	100	93.2	112 ± 3	8.15E-3 ± 1.01E-3	0.991	99.5
	150	126	155 ± 7	4.92E-3 ± 0.89E-3	0.981	365
	200	143	164 ± 5	6.89E-3 ± 1.05E-3	0.984	358
303	100	116	133 ± 4	7.72E-3 ± 1.12E-3	0.986	201
	150	147	163 ± 6	7.91E-3 ± 1.46E-3	0.975	535
	200	173	184 ± 6	1.11E-2 ± 0.23E-2	0.966	976
313	100	131	159 ± 7	5.23E-3 ± 1.01E-3	0.977	456
	150	167	191 ± 6	6.13E-3 ± 0.92E-3	0.984	478
	200	189	203 ± 8	8.50E-3 ± 1.98E-3	0.958	145
Elovich						
T (K)	C_0 (mg L^{-1})	$q_{e(exp)}$ (mg g^{-1})	A	B	R^2	SSE
293	100	93.2	54.6 ± 1.8	22.8 ± 1.4	0.977	248
	150	126	71.2 ± 3.0	30.7 ± 2.3	0.962	729
	200	143	89.1 ± 2.3	31.0 ± 1.7	0.982	401
303	100	116	69.4 ± 1.8	25.3 ± 1.4	0.981	267
	150	147	120 ± 3	30.8 ± 2.2	0.978	622
	200	173	92.4 ± 2.2	30.0 ± 17	0.982	395
313	100	131	76.4 ± 3.1	30.7 ± 2.4	0.961	779
	150	167	104 ± 3	36.2 ± 2.3	0.977	701
	200	189	127 ± 3	34.8 ± 2.4	0.978	763

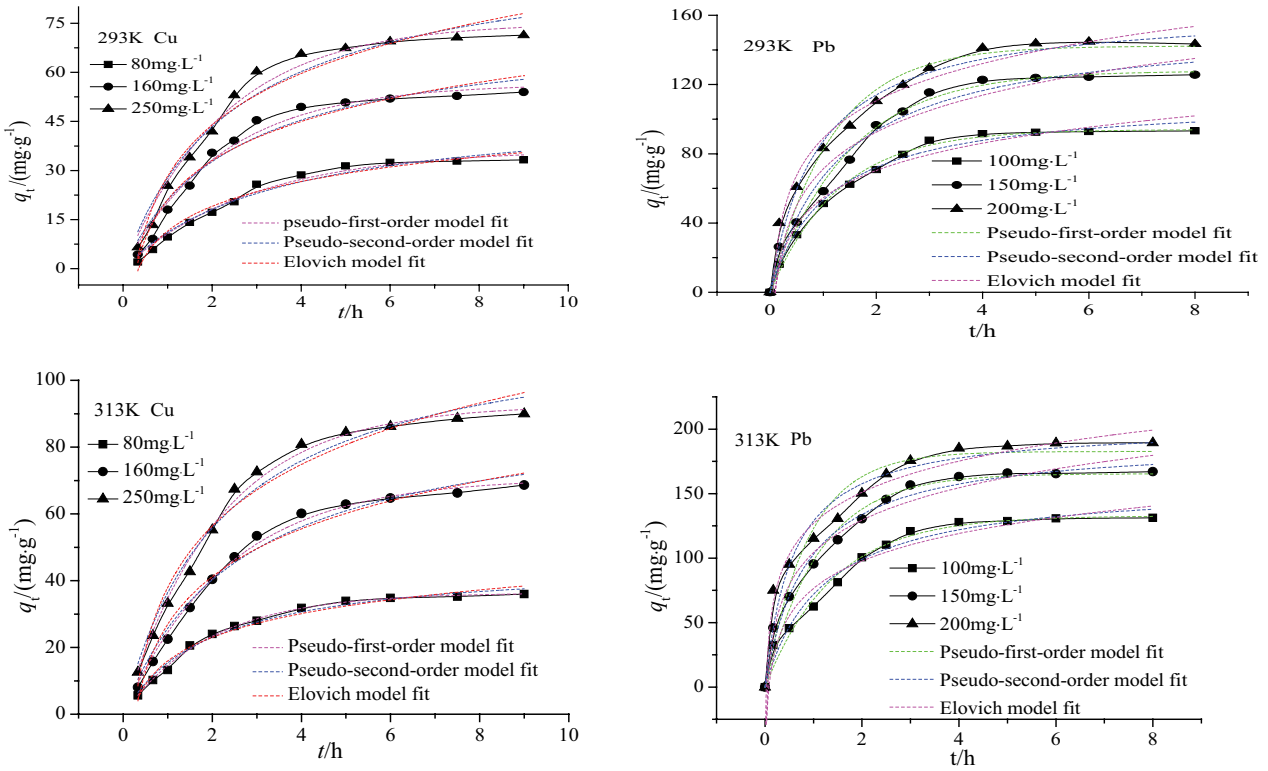

Fig. S1. Adsorption kinetics (293 K and 313 K) of Cu(II) and Pb(II) adsorption on PVDF-PEI.

Table S5
Comparison of PVDF-PEI and general adsorbents in adsorption performance

Adsorbent	Adsorbate	t (h)	pH	q_e (mg g^{-1})	References
Magnetic chitosan nanopowder		1	5.5	92.34	[S1]
Biowaste-derived char@SiO_2-NH_2		24	6	30	[S2]
Cu(II)-imprinted poly(vinyl alcohol)/ poly(acrylic acid) membrane	Cu(II)	4	5.0	82.2	[S3]
N-Acetyl-L-cysteine-functionalized lignin		2	6.0	68.7	[S4]
PN-Fe_3O_4-IDA		3	5	47.7	[S5]
PVDF-PEI		4	5.2	95.0	This study
Magnetic composite microgel		24	5.0	45	[S6]
Magnetic chitosan nanopowder		1	5.5	113.4	[S1]
Sulfur-doped graphitic carbon nitride nanosheets		3	4.5	52.63	[S7]
Ceria nanoparticles	Pb(II)	1	6.2	142.8	[S8]
Fe_3O_4@DAPF core-shell ferromagnetic nanorods		1	5.0	83.3	[S9]
PBC@SiO_2-NH_2		24	5	120	[S2]
PN-Fe_3O_4-IDA		3	5	74.5	[S5]
PVDF-PEI		4	5.0	193	This study

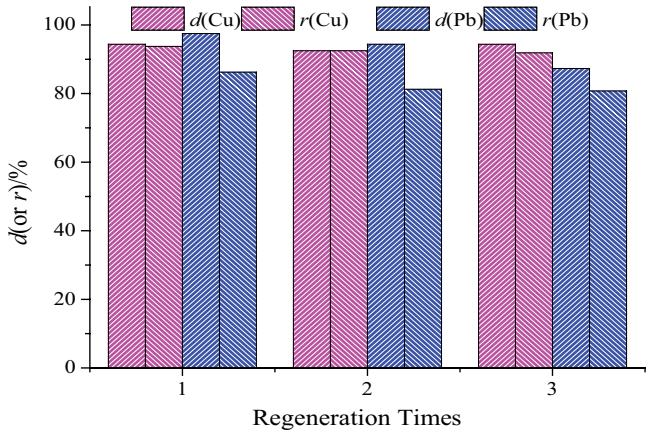

Fig. S2. Desorption regeneration research of Cu(II) and Pb(II).

References

[S1] S.Y. Pu, Y.Q. Hou, C. Yan, H. Ma, H.Y. Huang, Q.Q. Shi, S. Mandal, Z.H. Diao, W. Chu, *In situ* coprecipitation formed highly water-dispersible magnetic chitosan nanopowder for removal of heavy metals and its adsorption mechanism, ACS Sustainable Chem. Eng., 6 (2018) 16754–16765.

[S2] Y.L. Liu, J. Xu, Z. Cao, R.Q. Fu, C.C. Zhou, Z.N. Wang, X.H. Xu, Adsorption behavior and mechanism of Pb(II) and complex Cu(II) species by biowaste-derived char with amino functionalization, J. Colloid Interface Sci., 559 (2020) 215–225.

[S3] J.S. He, J.P. Chen, Cu(II)-imprinted poly(vinyl alcohol)/ply(acrylic acid) membrane for greater enhancement in sequestration of copper ion in the presence of competitive heavy metal ions: material development, process demonstration, and study of mechanisms, Ind. Eng. Chem. Res., 53 (2014) 20223–20233.

[S4] C. Jin, X.Y. Zhang, J.N. Xin, G.F. Liu, J. Chen, G.M. Wu, T. Liu, J.W. Zhang, Z.W. Kong, Thiol–ene synthesis of cysteine-functionalized lignin for the enhanced adsorption of Cu(II) and Pb(II), Ind. Eng. Chem. Res., 57 (2018) 7872–7880.

[S5] A.A. Aryee, F.M. Mpatani, Y.Y. Du, A.N. Kani, E. Dovi, R.P. Han, Z.H. Li, L.B. Qu, Fe_3O_4 and iminodiacetic acid modified peanut husk as a novel adsorbent for the uptake of Cu(II) and Pb(II) in aqueous solution: characterization, equilibrium and kinetic study, Environ. Pollut., 268 (2021) 11572.

[S6] L.P. Jiang, P. Liu, Novel magnetic fly ash/poly(acrylic acid) composite microgel for selective adsorption of Pb(II) ion: synthesis and evaluation, Ind. Eng. Chem. Res., 53 (2014) 2924–2931.

[S7] X. Li, J.L. Xing, C.L. Zhang, B. Han, Y.H. Zhang, T. Wen, R. Leng, Z.H. Jiang, Y.J. Ai, X.K. Wang, Adsorption of lead on sulfur-doped graphitic carbon nitride nanosheets: experimental and theoretical calculation study, ACS Sustainable Chem. Eng., 6 (2018) 10606–10615.

[S8] R. Sharma, S. Raghav, M. Nair, D. Kumar, Kinetics and adsorption studies of mercury and lead by ceria nanoparticles entrapped in Tamarind powder, ACS Omega, 3 (2018) 14606–14619.

[S9] S. Venkateswarlu, M. Yoon, Core-shell ferromagnetic nanorod based on amine polymer composite (Fe_3O_4@DAPF) for fast removal of Pb(II) from aqueous solutions, ACS Appl. Mater. Interfaces, 7 (2015) 25362–25372.